Journal of Catalysis **206,** 218–229 (2002)
doi:10.1006/jcat.2001.3432, available online at http://www.idealibrary.com on IDEAL®

Reduction of Prostaglandin Unsaturated Ketones to Secondary Allylic Alcohols by Hydrogen Transfer over Mesoporous-Supported PtSn Catalysts

Simona N. Coman,* Vasile I. Parvulescu,* Mario De Bruyn,† Dirk E. De Vos,† and Pierre A. Jacobs†,[1]

*University of Bucharest, Faculty of Chemistry, Department of Chemical Technology and Catalysis, Bdul Regina Elisabeta 4-12, Bucharest 70346, Romania; and †Katholieke Universiteit Leuven, Centre for Surface Chemistry and Catalysis, Kasteelpark Arenberg 23, B-3001 Leuven, Belgium

Received June 4, 2001; revised September 17, 2001; accepted September 28, 2001

Supported PtSn catalysts were prepared by successive impregnation of SiO_2, MCM-41, or MCM-48 materials with Pt and Sn, followed by calcination and reduction. The oxidation and aggregation state of the Pt and Sn were studied using combined temperature-programmed reduction, X-ray photoelectron spectroscopy, X-ray diffraction, and transmission electron microscopy experiments. The characteristics of the bimetallic catalysts were related to the catalytic behavior in the hydrogen transfer reduction of the unsaturated ketone moiety in some intermediates of the prostaglandin synthesis; isopropanol was used as the reductant. High chemoselectivities to the allylic alcohol (over 95%) were obtained with catalysts containing 5 wt% Pt and 5–10 wt% Sn on MCM-41 or MCM-48. Characterization of these optimum catalysts evidenced that most of the Pt and part of the Sn form supported alloy particles with PtSn and $PtSn_2$ composition; the rest of the Sn is present as dispersed $Sn^{2+/4+}$. Activation of the carbonyl group on oxidized Sn, steric shielding of the C=C bond by bulky substituents, and use of the hydrogen transfer donor seem crucial for obtaining high allylic alcohol chemoselectivities. In some cases, the mesoporous texture of the support induces significant diastereoselectivity, with one isomer of the secondary allylic alcohol prevailing over its epimer.

Key Words: **PtSn catalysts; MCM-41; MCM-48; hydrogen transfer reduction; prostaglandin intermediates; allylic alcohol.**

INTRODUCTION

Hydrogenation of unsaturated carbonyl compounds to saturated ketones or aldehydes is easily achieved over most platinum group metal catalysts under mild conditions and in different solvents. However, the selective hydrogenation of unsaturated carbonyl compounds to unsaturated alcohols still remains an important challenge for heterogeneous catalysis. This hydrogenation is a priori more difficult because the saturated carbonyl compound is much more stable as a final product. Several suitable catalytic systems have been reported for reduction of an unsaturated aldehyde to a primary allylic alcohol (1–20). These systems often contain an easily reducible metal of group VIII, and another oxidic compound, which is less easily reduced. Examples of such bimetallic systems are (Pt, Rh, Ru)–(Sn, Fe, Mn) species, supported on conventional silica, alumina, zeolites, or active carbon. Among these, PtSn has attracted most interest because of the high intrinsic chemoselectivities. Several attempts were made to identify the factors that control the selectivity in hydrogenation of unsaturated carbonyl compounds. Frequently invoked factors are electronic effects (21), shape selectivity (22), and adsorption on Lewis acid sites (23). For instance, in the specific case of gas-phase crotonaldehyde hydrogenation, the high $S_{C=O}$ selectivities are attributed to the formation of ionic tin. Using Mössbauer spectroscopy, Margitfalvi *et al.* (24, 25) showed that Sn^{4+} is formed at the surface of supported PtSn nanoclusters by "reaction-induced" activation, namely by transfer of oxygen from the reagents to tin (26). However, inspection of the literature shows that there are few reports on the heterogeneously catalyzed synthesis of secondary allylic alcohols via reduction of unsaturated ketones.

A possible solution to this chemoselectivity problem may be found in the hydrogen-transfer approach, which uses an organic molecule as a reductant instead of H_2 (27–31). Typical reducing reagents are unsaturated hydrocarbons such as cyclohexene or cyclohexadiene, primary or secondary alcohols such as methanol, benzyl alcohol, or 2-propanol, and formic acid. We have focused our interest on the reduction of unsaturated ketones, using a prostaglandin intermediate containing the enone moiety as a model substrate. Prostaglandins have numerous physiological roles, and they consequently have widely varying pharmaceutical applications (32). Synthetic analogues of prostaglandins have been developed with the aim of obtaining compounds that are more stable and have longer duration of action and a more specific effect. For instance, Cloprostenol is a synthetic analogue of prostaglandin $F_{2\alpha}$ (Scheme 1); it is used as a luteolitic agent in veterinary medicine. One of the

[1] To whom correspondence should be addressed. Fax: 32 16 32 1998. E-mail: pierre.jacobs@agr.kuleuven.ac.be.

0021-9517/02 $35.00

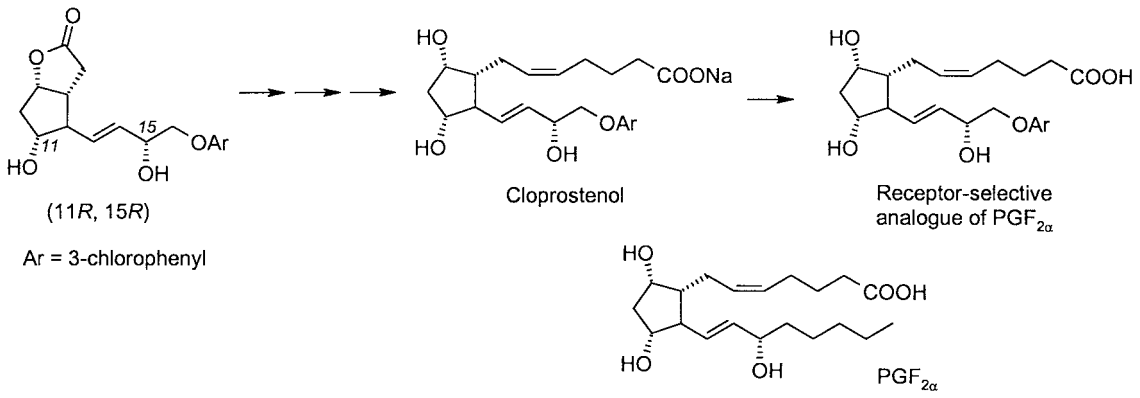

SCHEME 1

synthesis steps of Cloprostenol involves the diastereoselective reduction of the C=O bond with a C=C bond in the α position (substrate **1** in Scheme 2). The reduction can lead to a mixture of diastereomers, as depicted in Scheme 2; however, only the 15*R* form of the allylic alcohol (Scheme 2, substrate **2**) exhibits biological activity and hence has practical importance (note that the atom numbers 11 and 15 refer to the structure of $PGF_{2\alpha}$).

The present work reports on the performances of PtSn catalysts, supported on SiO_2, mesoporous MCM-41, or MCM-48, in hydrogen transfer reduction of the lactonic enone intermediate 1 ([3aα,4α(E),5β,6aα]-(±)-4-[4-(3-chlorophenoxy)-3-oxo-1-butenyl]-hexahydro-5-hydroxy-2H-cyclopenta[b]-furan-2-one) (Scheme 2) in the synthesis of the commercial drug Cloprostenol. Since the state of Pt and Sn in bimetallic catalysts is known well to depend on such things as the metal precursor, the support, and the precise pretreatments, the catalysts were characterized using several techniques. It is demonstrated that with some catalysts, almost perfect chemoselectivity for the allylic alcohol can be obtained. Relations between the catalytic observations and the physical state of Sn and Pt are discussed. We previously reported on a similar reaction using formic acid as a hydrogen donor instead of 2-propanol (33); however, as is demonstrated, results are far superior with 2-propanol.

EXPERIMENTAL

Silica (Degussa, FK 310, $S_{sp} = 200$ m^2/g), MCM-41 ($S_{BET} = 935$ m^2/g), and MCM-48 ($S_{BET} = 1317$ m^2/g) were used as supports for bimetallic catalysts. The MCM-41 support was prepared in a TEAOH medium using LUDOX AS-40 (Du Pont, 40 wt% colloidal silica in water) and cetyl trimethylammoniumchloride as a template (34). The MCM-48 was prepared according to a literature reference (35). Average pore diameters, as determined by N_2 adsorption using the Barrett–Joyner–Hallender calculation, were

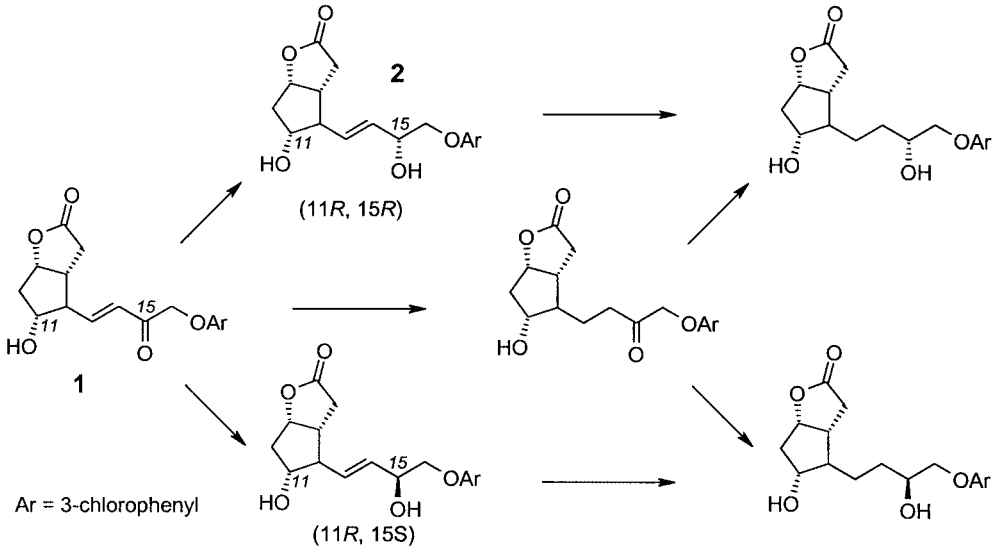

SCHEME 2

TABLE 1

Pt and Sn Loadings and Pt/Sn Molar Ratios of the Different Catalysts Prepared

Catalyst	Pt (wt%)	Sn (wt%)	Sn/Pt molar ratio
5% Pt on SiO_2, MCM-41 or MCM-48	5	—	—
5% Pt–1% Sn on SiO_2, MCM-41 or MCM-48	5	1	0.33
5% Pt–3% Sn on SiO_2, MCM-41 or MCM-48	5	3	0.99
5% Pt–5% Sn on SiO_2, MCM-41 or MCM-48	5	5	1.63
5% Pt–10% Sn on SiO_2, MCM-41 or MCM-48	5	10	3.23
5% Pt–15% Sn on SiO_2, MCM-41 or MCM-48	5	15	5.00
5% Sn on SiO_2, MCM-41 or MCM-48	—	5	—

27 Å for MCM-41 and 24 Å for MCM-48. Both molecular sieves were calcined at 813 K for 10 h. Prior to impregnation, silica was also dried and calcined at 773 K for 4 h. PtSn supported catalysts were prepared via a two-step procedure, using the incipient wetness technique. Before impregnation, the wetting capacity was measured by water titration of the calcined supports. All supports used exhibited a very similar water-adsorption capacity (7 ml of water g^{-1} of support). First, Pt was introduced by contacting 1 g of calcined support with an aqueous solution of $[Pt(NH_3)_4]Cl_2$ (Aldrich) (0.0901 g complex in 7 ml of water). The samples were then dried at 333 K for 4 h. Tin was introduced in the second step. Different amounts of $SnCl_2 \cdot 2H_2O$ were dissolved at room temperature in 7 ml of ethanol to obtain the Sn loadings indicated in Table 1. After the tin deposition, the catalysts were dried for another 2 h at 333 K, calcined in air flow at 673 K (5 ml min^{-1} for 4 h, with a heating rate of 2 K min^{-1}), and reduced in hydrogen flow (30 ml min^{-1} at 673 K for 1 h). Chemical analysis performed by inductively coupled plasma–atomic emission spectroscopy indicated the same Pt loading (5 wt%) for all the investigated catalysts, while the amount of tin varied between 0 and 15 wt% (Table 1). For comparison, 5 wt% Sn/support and 5 wt% Pt/support catalysts were also prepared.

The mesoporous sieves were characterized by adsorption –desorption of N_2 at 77 K. The catalysts were characterized using X-ray diffraction (XRD), X-ray photoelectron spectroscopy (XPS), H_2 temperature-programmed reduction (TPR), and transmission electron microscopy (TEM). Adsorption and desorption isotherms of N_2 at 77 K were recorded with a Coulter Omnisorp 100 CX apparatus. Prior to the measurements, the samples were outgassed overnight at 673 K under vacuum. The XPS spectra were recorded using a SSI X-probe FISONS spectrometer (SSX-100/206) with monochromated AlK_α radiation. The spectrometer energy scale was calibrated using the Au $4f_{7/2}$ peak. For the calculation of the binding energies, the C 1s peak of the C-(C, H) component at 284.5 eV was used as an internal standard. The peaks assigned to the Pt $4f_{7/2}$, Sn $3d_{5/2}$, and Si 2p levels were quantitatively analyzed. All samples were reduced before the XPS measurements. To avoid a reoxidation of the metallic species, these samples were kept under heptane and the XPS preparation procedures were performed in heptane. XRD patterns were recorded using a SIEMENS D5000 Matic diffractometer. The diffractograms were recorded between 2 and 65° 2θ at a scanning speed of 1 K/min, using the CuK_α radiation. H_2 TPR experiments were carried out with a temperature-programmed desorption/TPR 2705 instrument, 027 Pulse Chem Sorb option (Micromeritics). All the experiments were carried out with a constant flow rate of 0.79 $cm^3\ s^{-1}$ and a hydrogen concentration of 2.05 μmol cm^{-3} in an argon–hydrogen mixture. For the TEM investigations the catalytic material was placed on a specially produced, structureless carbon support film with a thickness of only 4 nm. These thin support films are stable enough for covering copper grids with a mesh width of 60 μm without an additional holey organic film. The powder was suspended in ethanol using an ultrasonic method. A drop of this suspension was placed on the support film and after 1 min the remaining unadsorbed solution was removed. The electron microscopy was carried out on a Siemens Elmiskop 102. An electron magnification of 50,000 : 1 was sufficient for the deduction of all significant structural details.

Catalytic tests were carried out in glass vials, at 353 K, under vigorous stirring, using 2 g of 2-propanol as solvent and hydrogen donor. The amount of catalyst was 25 mg and the amount of prostaglandin 14 mg. All the catalytic tests used freshly reduced catalysts. The prostaglandin precursor **1** as well as reference reaction products for chromatographic analysis were a gift from Dr. F. Cocu (Chemical and Pharmaceutical Research Institute, Bucharest, Romania). Reaction products were intermittently withdrawn from the glass vials and analyzed in a high performance liquid chromatography system with a SUPELCOSIL LC-18 column, an eluent containing water and acetonitrile in a 70 : 30 volume ratio, a pressure of 13.0–13.2 MPa, and a flow of 1.0 ml min^{-1}.

RESULTS

X-Ray Diffraction

XRD before and after deposition of the metals shows that the mesoporous structure of the support remains intact during catalyst calcination and reduction. In the case of MCM-41, four peaks are observed in the low 2θ region, corresponding to d-spacings of d_{100} = 3.932 nm, d_{110} = 2.287 nm, d_{200} = 1.977 nm, and d_{210} = 1.499 nm. These peaks are characteristic for the hexagonal structure (34).

Since MCM-41 is not crystalline at the atomic level, no reflections were observed at higher angles. The XRD pattern of MCM-48 indicates a structural order for the cubic crystallographic space group Ia 3d (d_{211} = 3.528 nm, d_{220} = 3.067 nm, d_{321} = 2.328 nm, d_{400} = 2.162 nm, d_{420} = 1.919 nm, and d_{332} = 1.841 nm) (35).

Figure 1 shows some XRD patterns of reduced PtSn catalysts. For MCM-41 and MCM-48, the d-spacings in the low-angle domain were unaltered, indicating that the hexagonal or cubic structures do not undergo major modifications by the metal deposition. With increasing Sn content, the XRD characteristics show clear changes, as indicated on the XRD patterns, but these changes are somewhat dependent on the support used (36–38). In the absence of Sn, or at low Sn contents (1%), only peaks of metallic Pt are observed. In some cases these lines are quite weak, indicating that the Pt is present in a dispersed, almost X-ray invisible state. Upon increasing the Sn content, diffraction lines of platinum–tin alloys become apparent. For instance, a sample with 5% Pt and 3% Sn on MCM-41 clearly contains Pt_3Sn, together with metallic Pt. A PtSn alloy with niggliite pattern is generally observed at intermediate Sn contents (i.e., between 5 and 10% Sn). Finally, at high Sn contents (10–15 wt%), Sn-rich alloy phases become observable (e.g., $PtSn_2$ (39) or even Pt_2Sn_3 (40) in 5% Pt–10% Sn/MCM-48). For reduced bimetallic samples on the SiO_2 support (data not shown in Fig. 1), the observed phases are the same as for PtSn on MCM-41, except for 5% Pt–1% Sn/SiO_2 (metallic Pt and Pt_3Sn alloy) and 5% Pt–15% Sn/SiO_2 ($PtSn$ and $PtSn_2$ alloys).

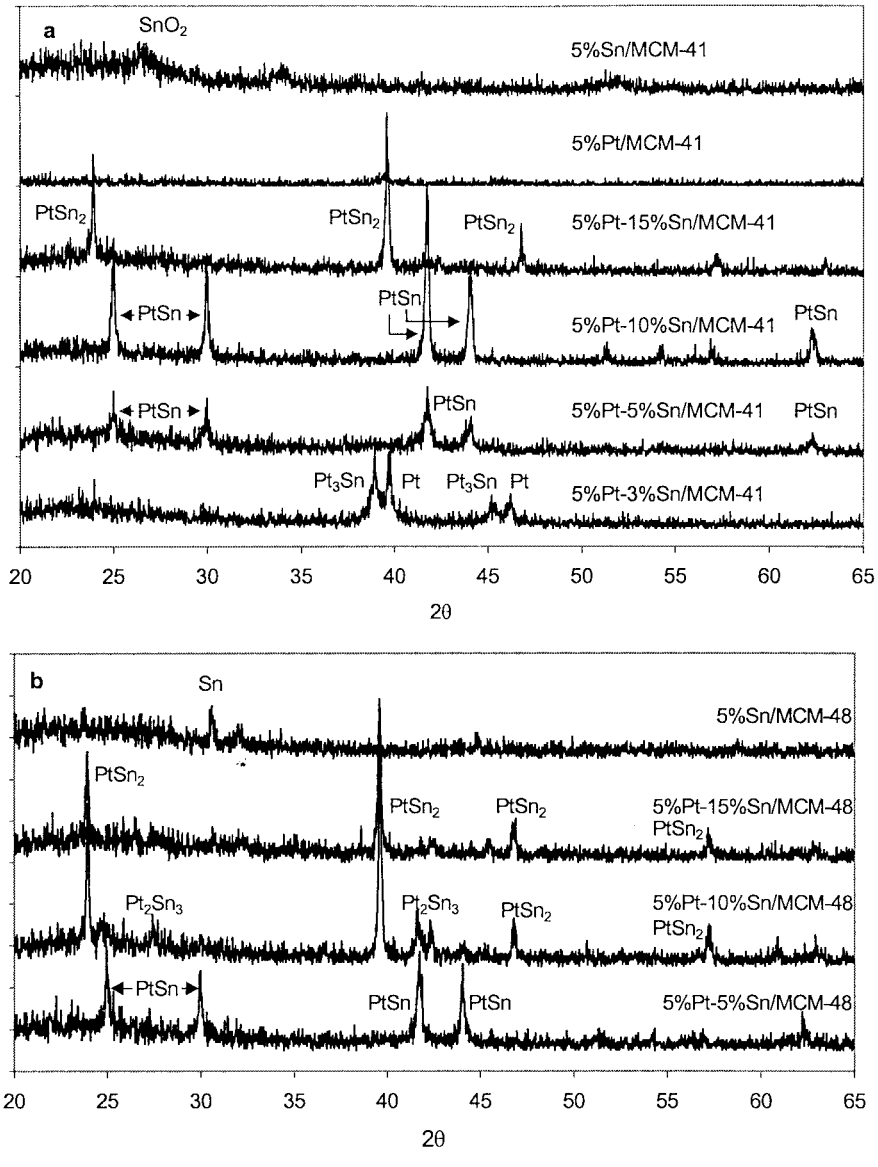

FIG. 1. XRD patterns for PtSn catalysts: (a) on MCM-41, (b) on MCM-48.

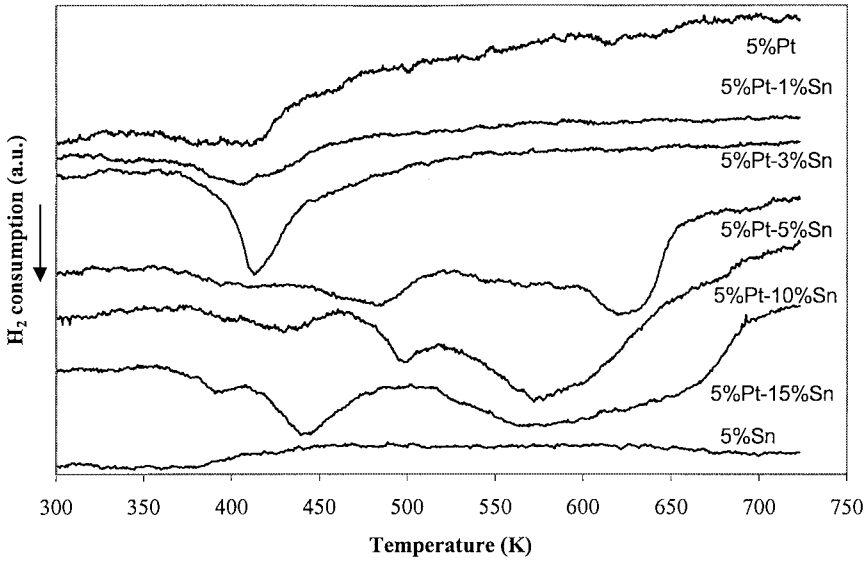

FIG. 2. H_2 TPR profiles for PtSn/MCM-41 catalysts.

For completeness, some diffractograms of Pt-free materials are included. These contain weak lines (e.g., of SnO_2) for 5% Sn/MCM-41, and of metallic Sn for 5% Sn/MCM-48. Thus it seems that even in the absence of Pt, Sn may be reduced to some extent, even if this XRD-observable Sn may only constitute a small fraction of the total Sn.

Hydrogen Temperature Programmed Reduction

Figure 2 compiles the H_2 TPR data for calcined PtSn/MCM-41 catalysts. Clearly an increasing Sn content strongly affects the qualitative and quantitative characteristics of the reduction profile (41).

The reduction in a monometallic 5% Pt/MCM-41 catalyst takes place largely in mild conditions, at temperatures below 423 K. This means that most of the platinum oxide interacts only weakly with the support. For a catalyst with only tin, there is hardly any reduction, at least in the temperature domain considered (293–723 K). Apparently reduction of isolated Sn requires higher temperatures.

Bimetallic samples with low Sn contents, such as 5% Pt–1% Sn/MCM-41 and 5% Pt–3% Sn/MCM-41 are largely reduced below 423 K. The slight shift of the peak maximum can be related to the formation of new alloy-type surface species. Indeed, comparison with the XRD data shows that this reduction should form not only Pt but also Pt_3Sn species.

At higher Sn contents, the amount of H_2 consumed clearly increases. This means that not only Pt but also Sn is to a considerable extent reduced, as was already inferred from the XRD data. Moreover, the profiles become complex, with important H_2 consumption at low temperatures (below 473 K) and at high temperatures (between 523 and 673 K). The TPR peak at 613 K observed in the case of the 5% Pt–5% Sn sample can be found in the other catalysts with a high tin content, but it overlaps with other peaks below and above this temperature. The low-temperature components probably correspond to initial formation of Pt metal or Pt-rich alloys; the high-temperature reductions correspond to massive reduction of Sn by incorporation into platinum–tin alloys. Clearly, higher Sn concentrations facilitate the formation of Sn alloys such as PtSn and $PtSn_2$.

To summarize, addition of small amounts of Sn shifts Pt reduction to slightly higher temperatures and forms Pt-rich alloys; in Sn-rich samples, there is a broad shoulder at low temperatures (below 613 K) but a high-temperature reduction is also observed, consistent with the formation of new PtSn alloys. Similar behavior was recorded for silica- and MCM-48-supported samples.

Electron Microscopy

The mesoporous support materials and the mono- and bimetallic catalysts were also characterized using TEM. The typical mesoporous structure was not damaged during the metal deposition and activation steps. The deposition of Sn alone does not lead to TEM-observable particles; this is in agreement with the absence or very low intensity of XRD lines in samples containing only Sn. In bimetallic samples, metal clusters were clearly observed. The largest metal particles have a diameter of 15–20 nm, but the major number fraction has a diameter between 2 and 10 nm. For the mesoporous MCM-41 and MCM-48 supports, this implies that the smallest metal particles may reside inside the pores; however, the larger metal particles must have migrated outside the mesopores to the outer surface.

TABLE 2

XPS Binding Energies, XPS, and Overall Elemental Ratios for PtSn Catalysts with SiO_2, MCM-41, and MCM-48 Supports

Support	5% Pt	5% Pt–1% Sn	5% Pt–3% Sn	5% Pt–5% Sn	5% Pt–10% Sn	5% Pt–15% Sn	5% Sn
SiO_2							
Binding energy, eV (Si 2p)	103.4	103.4	103.6	103.4	103.4	103.5	103.30
Binding energy, eV (Pt $4f_{7/2}$)	71.10	71.3	71.6	71.6	71.7	71.7	—
Binding energy, eV (Sn $3d_{5/2}$)	—	486.3	486.7	486.7	486.9	487.0	486.7
Pt/Si overall ratio	0.016	0.017	0.017	0.017	0.018	0.020	—
Pt/Si XPS ratio	0.005	0.006	0.012	0.009	0.009	0.013	—
Sn/Si overall ratio	—	0.005	0.016	0.028	0.059	0.095	0.026
Sn/Si XPS ratio	—	0.005	0.011	0.017	0.038	0.049	0.021
Sn/Pt overall ratio	—	0.33	0.99	1.63	3.23	5.0	—
Sn/Pt XPS ratio	—	0.72	0.97	1.96	4.35	3.85	—
MCM-41							
Binding energy, eV (Si 2p)	103.8	103.9	103.7	103.9	103.9	103.9	103.9
Binding energy, eV (Pt $4f_{7/2}$)	71.4	71.7	71.9	71.8	71.8	72.0	—
Binding energy, eV (Sn $3d_{5/2}$)	—	486.3	486.5	486.6	486.9	486.9	487.3
Pt/Si overall ratio	0.016	0.017	0.017	0.017	0.018	0.020	—
Pt/Si XPS ratio	0.006	0.006	0.008	0.005	0.005	0.006	—
Sn/Si overall ratio	—	0.005	0.016	0.028	0.059	0.095	0.027
Sn/Si XPS ratio	—	0.004	0.008	0.009	0.017	0.025	0.025
Sn/Pt overall ratio	—	0.33	0.99	1.63	3.23	5.0	—
Sn/Pt XPS ratio	—	0.70	1.03	1.82	3.45	4.54	—
MCM							
Binding energy, eV (Si 2p)				103.56	103.42	103.87	103.57
Binding energy, eV (Pt $4f_{7/2}$)				72.1	72.0	72.1	—
Binding energy, eV (Sn $3d_{5/2}$)				486.4	487.0	486.9	487.0
Pt/Si overall ratio				0.017	0.018	0.020	—
Pt/Si XPS ratio				0.007	0.009	0.003	—
Sn/Si overall ratio				0.028	0.059	0.095	0.027
Sn/Si XPS ratio				0.023	0.048	0.066	0.032
Sn/Pt overall ratio				1.64	3.23	5.0	—
Sn/Pt XPS ratio				3.57	5.55	19.45	—

X-Ray Photoelectron Spectroscopy

Table 2 shows binding energies for the photoelectron peaks of Pt $4f_{7/2}$, Sn $3d_{5/2}$, and Si 2_p in PtSn catalysts after reduction at 673 K. Elemental ratios, as obtained from the overall chemical composition and from XPS, are given in the same table. It is important that the chloride content of the catalyst surface was in all cases below the XPS detection limit, proving that the calcination effectively removes the C l ligands.

The XPS observation of the Pt $4f_{7/2}$ line shows a single, highly symmetric peak, whatever the support used. The average binding energy value of 71.7 ± 0.3 eV agrees with metallic Pt (42). The Pt binding energies are consistently slightly higher for bimetallic samples than for monometallic Pt samples; it is well-known that a higher dispersion or the presence of cations can increase the binding energy of metallic particles (43). Analysis of the Sn $3d_{5/2}$ line is less straightforward (6, 9, 42, 44–47). First, it is impossible to distinguish between Sn(II) and Sn(IV) by XPS. Second, the peak of pure Sn metal (484.6 eV) is normally well separated from that of oxidized Sn (486.9 eV), but in alloys, the Sn(0) peak seems to shift to higher values, resulting in a peak separation of only 1 eV (42). With the present samples, binding energies observed for the Sn species in reduced PtSn catalysts range from 486.3 to 487.3 eV (Fig. 3). The binding energy of the peak maximum is highest for samples with only Sn, or for samples with high Sn content (e.g., 5% Pt–15% Sn/MCM-41 or 5% Pt–10% Sn/SiO_2). It therefore

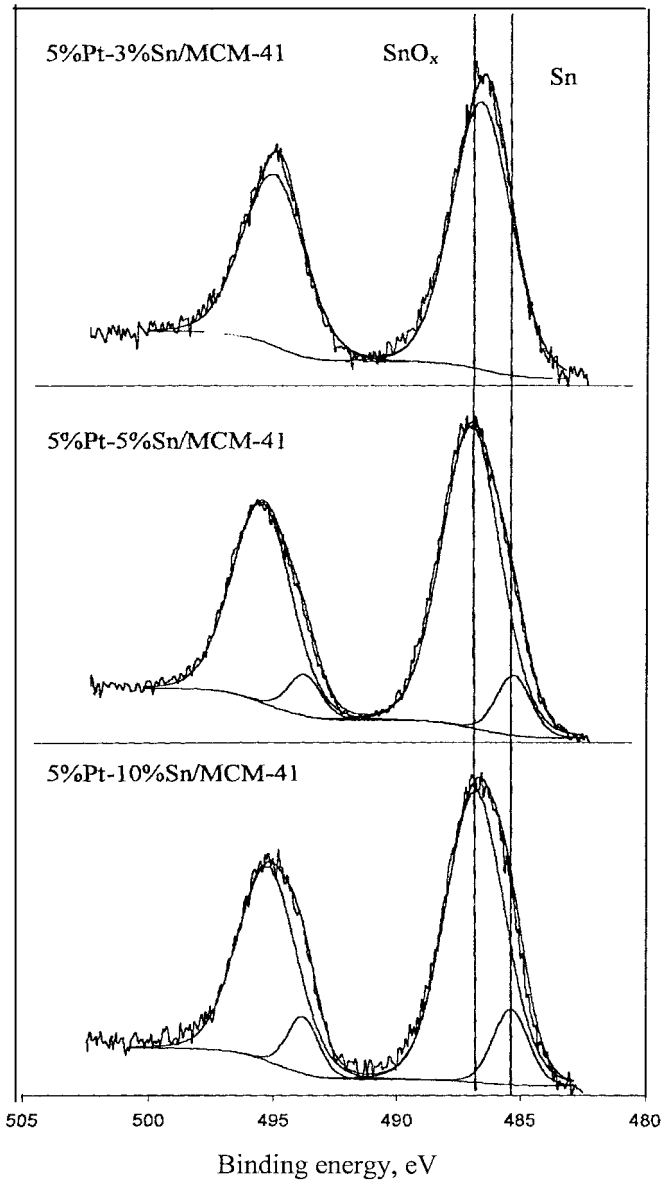

FIG. 3. Determination of the contribution of Sn^0 and oxidized Sn species to the XPS Sn $3d_{5/2}$ signal.

seems that oxidized Sn predominates at the catalyst surface. However, in the spectra of samples with a Sn content larger than 5%, there is a small contribution of alloyed Sn(0), as is evident from the slightly asymmetric peak shapes (Fig. 3). However, this Sn^0 seems to account for only 10% or less of the total Sn signal. Anyway, signals of isolated, monometallic Sn(0) are not observed.

Table 2 also shows values for Pt/Si, Sn/Si, and Sn/Pt atomic ratios, as determined by XPS, or alternatively derived from the stoichiometry of the preparation procedure (denoted by "overall" ratio). In samples containing only Sn, there is fair agreement between the XPS and overall Sn/Si ratios. This proves that the Sn is homogeneously distributed over the support; this is in agreement with XRD data, which showed no Sn oxide or Sn metal clusters. In the bimetallic samples, the overall and XPS Sn/Si ratios increasingly diverge as the Sn content increases. The rather low values of the XPS Sn/Si ratios at high Sn contents may be explained (i) by migration of Sn to the inner pore volume, or (ii) by incorporation of Sn in clusters that are too large to be completely probed by XPS. TEM analysis showed that in bimetallic PtSn catalysts part of the alloy particles have a diameter of 15–20 nm, which is quite larger than the expected XPS penetration depth of a few nanometers. As the latter particles cannot be accommodated in the (meso)pores, migration of Sn into these pores seems implausible. Therefore, the low Sn/Si XPS ratios in bimetallic catalysts must be due to a decreased dispersion of the Sn when it is incorporated in large alloy particles, (e.g., for 5% Pt–15% Sn/MCM-41 (48). At low tin content, both Pt and Sn are in a highly dispersed state, since no or very weak XRD patterns are observed. However, the similarity of the TPR curves of the 5% Pt and 5% Pt–1% Sn sample (Fig. 2) indicates that alloy-type bimetallic surface species have to be formed. These bimetallic surface species can be either small Pt_3Sn nanoclusters or Pt clusters having well-dispersed metallic tin in it.

The Pt/Si ratios are less easily interpreted. Generally, the XPS values are lower than the overall ratios, due to either intraporous concentration of Pt or to formation of large extraporous clusters. Finally, the Sn/Pt ratios are a complex result of the different aggregation behavior of the Pt and the Sn. For instance, in MCM-41, the Sn/Pt XPS ratio is higher than the overall ratio at low Sn contents; this indicates that Sn is more evenly distributed over the support than is Pt. For high Sn contents in the PtSn/MCM-41 catalysts, the differences between the XPS and overall Pt/Sn ratios are small.

Catalytic Experiments

The possible products of the hydrogen transfer reduction of prostaglandin intermediate 1 are shown in Scheme 2. The selectivity for the desired allylic alcohols may be decreased by a parallel reduction of the enone to the saturated ketone, or by a consecutive reaction of the allylic alcohol to the saturated alcohol.

SiO_2 catalysts. A monometallic Pt/SiO_2 catalyst shows a rather good conversion in the reaction but poor selectivity to the allylic alcohol (AA) (Table 3, first entry). The high selectivity for the saturated ketone demonstrates that the C=O hydrogenation only poorly competes with reaction at the C=C bond. The effect of different amounts of Sn is reported in Table 3. All the PtSn samples, except 5% Pt–1% Sn, were less active than was the monometallic sample, but displayed a higher chemoselectivity for the AA. An increase in the amount of tin to 15 wt% leads to a maximum of 31% chemoselectivity to AA for a conversion of 14.4%. The selectivity for AA is however still somewhat lower than the chemoselectivity for the saturated ketone (46%). In

TABLE 3

Conversion of the Unsaturated Ketone and Chemoselectivity (*S*) for Allylic Alcohol, Saturated Alcohol, and Ketone on $PtSn/SiO_2$ Catalysts

Catalyst	Conversion (%)	$S_{\text{allylic alcohol}}$ (%)	$S_{\text{saturated alcohol}}$ (%)	S_{ketone} (%)
5% Pt/SiO_2	32.2	4	22	74
5% Pt–1% Sn/SiO_2	16.0	0	61	39
5% Pt–3% Sn/SiO_2	16.8	11	48	41
5% Pt–5% Sn/SiO_2	7.3	14	73	13
5% Pt–10% Sn/SiO_2	16.8	28	36	36
5% Pt–15% Sn/SiO_2	14.4	31	23	46
5% Sn/SiO_2	25.1	80	14	6

Note. Reaction conditions: 25 mg of catalyst, isopropanol, 353 K, 48 h.

all cases, the reaction occurred without any diastereomeric excess, yielding racemic AA. The 5% Sn/SiO_2 is itself an active and chemoselective catalyst for this reaction, with an 80% AA selectivity at 25% conversion.

MCM-41-based catalysts. There are clear differences between the results obtained with MCM-41 and amorphous SiO_2 supports. First, with the monometallic 5% Pt-/MCM-41 catalyst, the substrate conversion is quite slow and results in an AA chemoselectivity of only 6% after a 72-h reaction. In Table 4, the conversions and the chemoselectivities to AA for all PtSn/MCM-41 catalysts are summarized. Table 4 and Fig. 4 show that Sn addition to these catalysts results in changes in activity, in particular in a large increase in AA chemoselectivity. On 5% Pt–10% Sn/MCM-41, the AA chemoselectivity reaches 93% at 20% conversion, with a diastereomeric excess of the 15*S* form of 20%. At very high Sn contents, the chemoselectivity decreases again, with values inferior to 70% for the 5% Pt–15% Sn/MCM-41 catalyst. For the latter material, the AA chemoselectivity increases during the reaction; this may be related to *in situ* "carbonyl activation" of some active sites during the hydrogenation reaction. This phenomenon, also known as reaction-induced selectivity improvement, has previously been described in the literature (24, 26). Major side products for the PtSn/MCM-41 catalysts are ketone, on 5% Pt–1% Sn/MCM-41 and 5% Pt–15% Sn/MCM-41, and saturated alcohol, for catalysts with intermediate Sn content (3–10%). The chemoselectivity trends as a function of Sn/Pt ratios, determined via XPS or based on preparation stoichiometry, are given in Fig. 5, together with the metallic phases observed using XRD. Again, the catalyst with only Sn (5% Sn/MCM-41) displays considerable activity, but the AA selectivity does not exceed 40%.

MCM-48-based catalysts. In terms of chemoselectivity to the AA, the use of the MCM-48 support was found to be even more advantageous than use of MCM-41. As in the case of the silica support, the 5% Pt/MCM-48 monometallic sample was very active, with complete conversion within 4 h, but the AA chemoselectivity is less than 5%. The addition of tin decreases the activity but increases the AA chemoselectivity. On 5% Pt–10% Sn/MCM-48 and 5% Pt–5% Sn/MCM-48, the AA selectivity is practically 100% at the beginning of the reaction and starts to decrease after 72 h because of further hydrogenation to the saturated

TABLE 4

The Variation of the Conversion and of the Selectivity to Allylic Alcohol (i-PrOH, 353 K) on PtSn(x = 1–15%)/MCM-41 Catalysts

	Conversion (%)						Selectivity (%)					
Time (h)	5% Sn	$x = 1$	$x = 3$	$x = 5$	$x = 10$	$x = 15$	5% Sn	$x = 1$	$x = 3$	$x = 5$	$x = 10$	$x = 15$
12	16	12.2	1.5	3	4.9	2.7	37	23.9	63.9	87.8	77.8	47.7
24	23.4	13	2.4	6	8.5	4.5	35.6	24.6	62.4	90.9	84.7	49.3
36	32	13.5	2.5	9	14	6.5	34.7	26.2	61.6	92.4	88.6	51.6
48	38.3	15	3.2	11.5	19.5	8.5	33.9	27.2	59.1	92.9	92.4	53.9
60	42	15	3.4	14.5	24.5	10	32.3	27.7	58.5	97	93.9	56.2
72	46.02	15.5	4.3	17.5	30	12.5	31.6	28.5	57.7	95.5	87	58.5
84	50	16	4.3	20	35	14.5	30.8	29.3	57	93.2	83.2	60.8
96	53	17.7	4.5	23.2	40	16.7	39.3	30	56.2	89.3	78.5	62.3
108	57	17.7	5.5	25.5	46.5	18	27.7	31.6	55.4	87.0	74.7	66.2
120	59.9	18.6	6.1	28.5	52	20	27.2	32.3	53.3	84.7	70.1	68.5
132	64	19	6.5	31.5	57	22.5	26.2	33.9	52.4	82.4	66.2	70.1
144	68	20	6.5	34.5	62.6	24	25.4	34.4	52.4	79.3	61.6	72.4

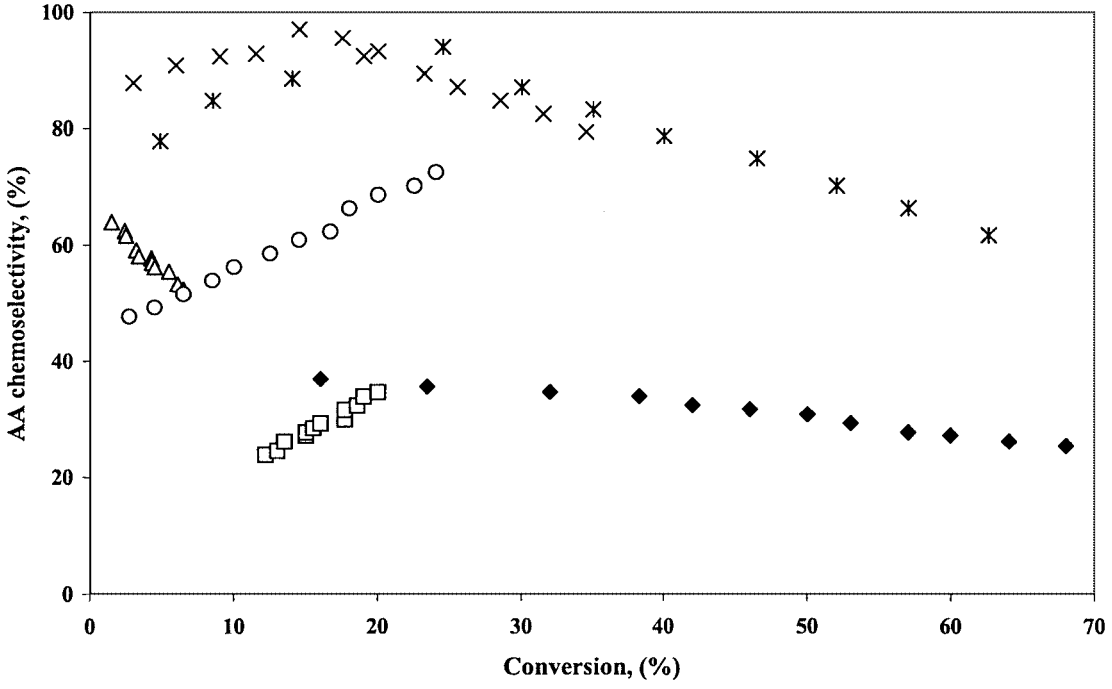

FIG. 4. The conversion–selectivity plot in the reduction of a prostaglandin enone over 5% Pt–*x*% Sn/MCM-41 catalysts: 5% Sn (◆), 5% Pt–1% Sn (□), 5% Pt–3% Sn (△), 5% Pt–5% Sn (x), 5% Pt–10% Sn (✱), 5% Pt–15% Sn (○) (i-PrOH, 353 K).

alcohol (Fig. 6). A large amount of Sn, as in 5% Pt–15% Sn/MCM-48, results after 72 h in 15% conversion with poor AA selectivity (9%). Finally, with 5% Sn/MCM-48, the maximum AA selectivity is 40%.

Diastereomeric excesses in the AA product. The variation of the diastereoselectivity in time, as a function of tin content and support nature, is shown in Fig. 7. For catalysts containing only Sn, or for the catalysts based on amorphous SiO_2 supports, no diastereomeric excess was observed. In contrast, significant excesses of the (11*R*, 15*S*) isomer are formed with the bimetallic mesoporous supports, particularly at the start of the reaction and at intermediate Sn

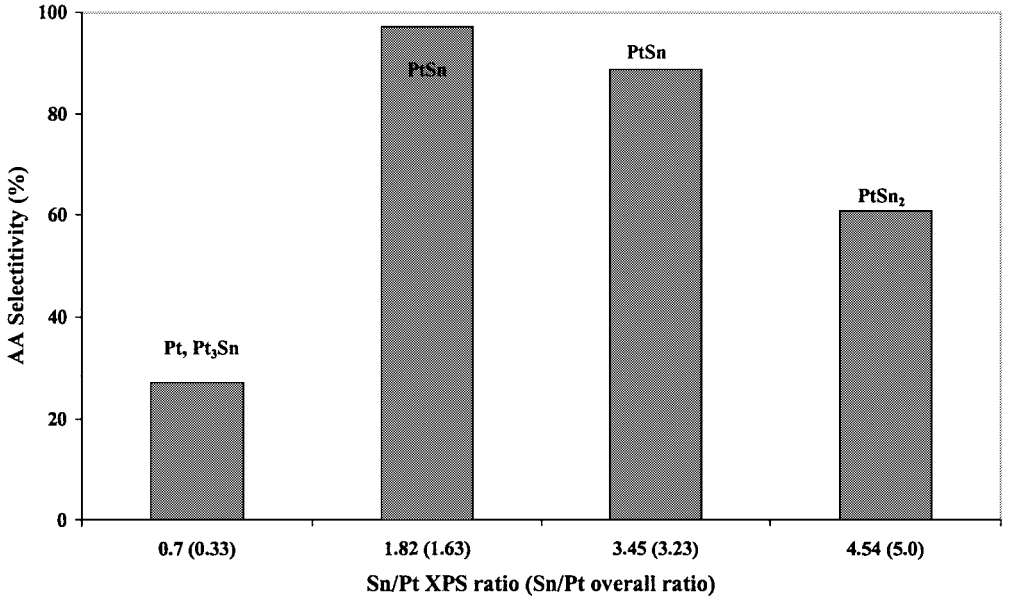

FIG. 5. The chemoselectivity to allylic alcohol (for a conversion of 15%) in the reduction of a prostaglandin enone over supported MCM-41 catalysts (i-PrOH, 353 K) as a function of the Sn/Pt XPS ratio and the overall Sn/Pt ratio (inside parentheses), together with the metallic phases observed in XRD.

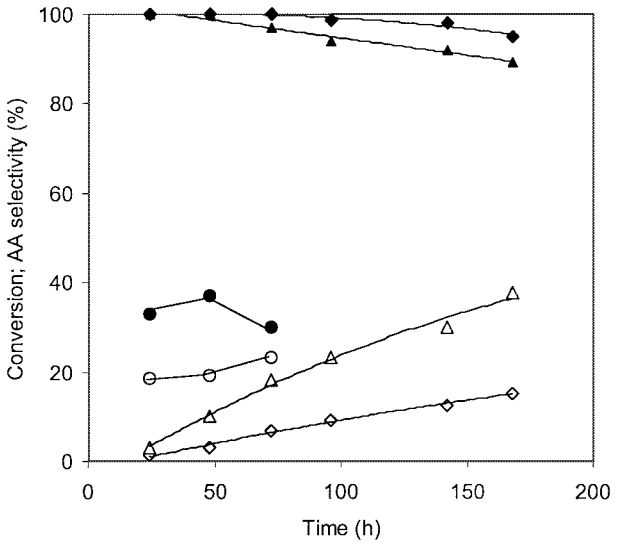

FIG. 6. Conversion (open symbols) and chemoselectivity to allylic alcohol (filled symbols) in hydrogen transfer reduction of a prostaglandin enone over Pt and Sn containing MCM-48 (i-PrOH; 353 K): 5% Pt–5% Sn (◆, ◇), 5% Pt–10% Sn (▲, △), 5% Sn (●, ○).

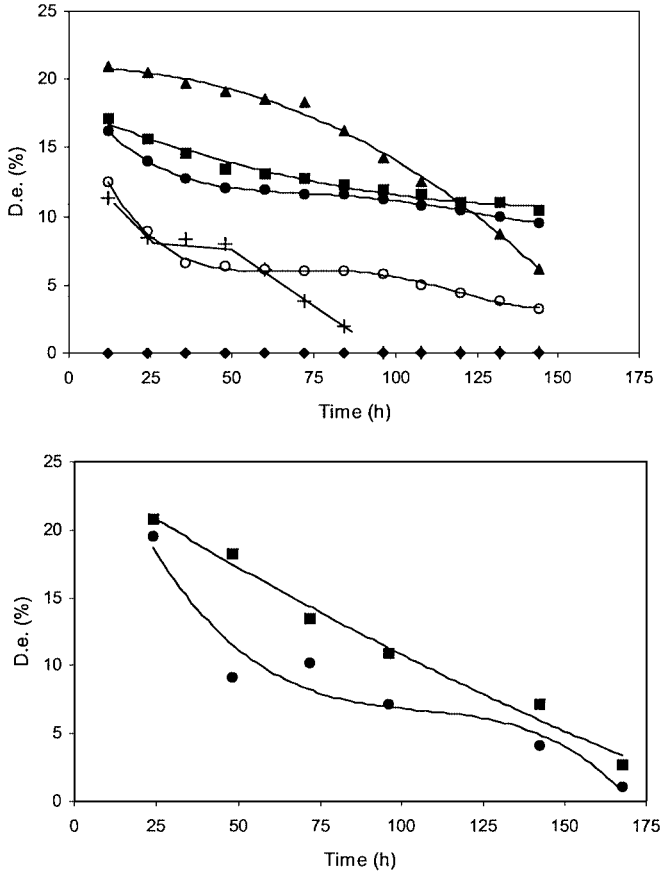

FIG. 7. Variation of the diastereoselectivity for the 11*R*, 15*S* configuration as a function of time for (top) MCM-41-supported catalysts, and (bottom) MCM-48-supported catalysts. 5% Sn (◆), 5% Pt–3% Sn (▲), 5% Pt–5% Sn (■), 5% Pt–10% Sn (●), 5% Pt–15% Sn (○), 5% Pt (+) (i-PrOH, 353 K).

contents (between 3 and 10 wt%). As the reaction time is increased, more of the (11*R*, 15*R*) epimer is formed, and the diastereomeric excess (de) gradually decreases.

DISCUSSION

The combination of four physicochemical techniques leads to a clear view on the nature of the supported Pt and Sn on the amorphous SiO_2 support, and on the mesoporous MCM-41 and MCM-48 supports. For the catalysts with only Sn, the pretreatment hardly leads to formation of metallic Sn, as evidenced by TPR and the XPS binding energy; the Sn(II) or Sn(IV) is finely divided over the support, as proven by TEM, XPS elemental ratios, and the absence of clear features in the XRD. Catalysts with only Pt contain, as expected, metallic Pt(0).

High Sn contents (10–15 wt%) provide a sufficient driving force for the formation of PtSn alloys, as evidenced by XRD and H_2 TPR, with particles large enough to be easily observed using TEM. Of all alloy phases observed, $PtSn_2$ has the highest tin content. However, overall Sn : Pt ratios in samples with 10 or 15 wt% Sn are 3.2 and 5, respectively. This means that even if all Pt is alloyed in $PtSn_2$, a large fraction of the Sn remains on the surface. Since Sn alone is not reduced on silica surfaces in the conditions employed, this residual Sn must be in the oxidized state. This is consistent with the binding energy in XPS, which gives proof for Sn(II) or Sn(IV) (42). Moreover, it is well-known that even very short air contacts or small contaminations lead to surface oxidation of metallic Sn or PtSn alloys (37). Alloys of Pt and Sn tend to be surface-enriched with Sn, because of the lower surface tension of Sn (37, 49). One can therefore expect that oxidized Sn covers to some extent the surface of the $PtSn_x$ alloy particles.

At low Sn contents (1–3 wt%), monometallic Pt^0 particles are the main reduced metal species, as evidenced by XRD. It is possible that a small amount of Sn is incorporated into these clusters in the form of alloy-type surface species.

The most salient fact in the catalytic results is that high AA chemoselectivities have been obtained in the hydrogenation of an unsaturated ketone. Indeed, the vast majority of the literature regarding work on doped Pt catalysts deals with unsaturated aldehydes such as acrolein, prenal, crotonaldehyde, or citronellal (1, 3, 4, 9, 15, 20, 24). Since in the present experiments isopropanol was used as a reductant instead of H_2, at least two mechanisms can lead to ketone hydrogenation.

1. A Sn-centered Meerwein–Ponndorf–Verley (MPV) mechanism can be considered. In this mechanism, the isopropanol reductant and the enone coordinate simultaneously on a Lewis acid center, followed by hydride transfer from isopropanol to the enone C=O group (50). Since the carbonyl function is selectively activated instead of the C=C double bond, one would expect substantial AA

selectivity. It is obvious that oxidized Sn species such as Sn^{4+} may display such activity; the reactions with Sn-only supported catalysts can reasonably be ascribed to MPV-type activity.

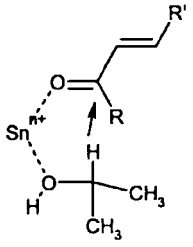

However, the experiments evidence that the use of Sn alone does not ensure high AA chemoselectivity; for instance with 5% Sn/MCM-41, the chemoselectivity amounts to only 40%. Clearly, while a Sn-centered MPV-type contribution cannot be excluded, it is not the only pathway. A possible explanation for the moderate and varying AA chemoselectivities with Sn-only catalysts may be that Lewis acid Sn^{n+} centers catalyze the isomerization of the AA to the saturated ketone. Since the Sn speciation may be different on the surfaces of SiO_2 and MCM materials, depending on the available silanol groups, this side reaction may occur to a different extent for the various Sn-only catalysts.

2. The reduction can be Pt-mediated. Chemisorbed H can be transferred from the metallic Pt or $PtSn_x$ surface to the carbonyl group; alternatively a metal-adsorbed donor molecule may transfer a hydrogen atom (28). Possible active species are sketched in below.

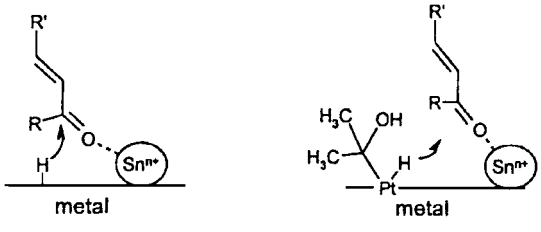

Particularly for the Pt-mediated mechanisms, the Sn doping is crucial, since virtually no AA selectivity is observed with Pt alone (the substrate conversion is quite slow and results in an AA chemoselectivity of only 6% after a 72-h reaction). For all chemoselective catalysts (e.g., 5% Pt–10% Sn/MCM-41 or on MCM-48), the physicochemical characterization gives firm evidence for the occurrence of PtSn metallic alloys *and* for the presence of an oxidized Sn species on the surface. Hence both alloying and the presence of oxidized Sn may play a role. Concerning the role of the Sn in the alloy particles, olefin C=C bonds are less strongly bonded on PtSn alloys in comparison with Pt alone (51). This way, the Sn favors adsorption of the C=O bond at the expense of C=C adsorption. Moreover, Sn admixture reduces the size of the Pt surface ensembles and thus may impede 1,4-adsorption, with simultaneous interaction of the C=C and the C=O double bonds with the surface. Such a 1,4-adsorption of the substrate in the first step may result in the formation of the enol, which by instantaneous isomerization will give the saturated ketone; the latter may then be further hydrogenated to the saturated alcohol instead of to the desired AA. A complementary role can be played by the Sn^{n+} cations on the surface: the carbonyl groups can coordinate to these ions (e.g., in a η^1 fashion) (26, 52). This increases the susceptibility of the carbonyl group to reduction, and due to the intimate mixing of the Pt and the Sn, such a coordinative bond brings the C=O group close to a surface. In proximity of the surface, the C=O group, activated on ionic Sn^{n+}, then reacts with surface-activated H atoms or with adsorbed H-transferring organic molecules.

At least two other factors can contribute to the unexpectedly high chemoselectivity in the enone reduction.

1. The C=C double bond in the enone group of the prostaglandin precursor **1** is subject to considerable steric hindrance, because of the presence of a substituted cyclopentyl group in α of the C=C bond (53).

2. The use of isopropanol instead of H_2 is indispensable for obtaining high chemoselectivities. In all reactions where we used H_2 instead of isopropanol with the same catalysts, the AA chemoselectivities were invariably very low. Mechanisms of noble-metal-mediated transfer reductions are very complex; not only surface-adsorbed H but also surface-adsorbed organic molecules may transfer hydrogen atoms to a substrate (28). Irrespective of the precise mechanism, it seems that there are several facts which make double hydrogenation to the saturated alcohol less likely: (i) low hydrogen coverage using isopropanol instead of H_2 (on such a low-coverage surface it is easier to limit the reaction to reduction of only one double bond); (ii) low mobility of hydrogen at the metallic surface; (iii) activation of the carbonyl group by Sn^{n+}; and (iv) suppression of the adsorption of the substrate with its olefinic double bond.

Finally, significant diastereomeric excesses were obtained with PtSn catalysts on ordered mesoporous supports. This indicates that interaction between metal particle, promoter, and substrate can proceed in a more-or-less ordered fashion when the supporting surface is uniform enough, or when the reaction takes place in the constrained environment of the mesopores of the MCM-41 or MCM-48 structures.

CONCLUSIONS

While research in the hydrogenation of C=C–C=O groups has mostly focused on unsaturated aldehydes, we here present an example of reduction of an unsaturated ketone to a secondary allylic alcohol using a PtSn catalyst. This is an unusual reaction, since unsaturated ketones (e.g., methyl vinyl ketone) usually only yield the saturated ketone or the saturated alcohol. In a recent review paper, Ponec even expressed doubts whether unsaturated ketones can

be at all selectively hydrogenated to allylic alcohols using group VIII catalysts (26).

Our results clearly prove that the answer to this question is positive and simultaneously indicate a number of important reaction variables. Our successful catalysts were MCM-type supports containing 5 wt% Pt and 5–10 wt% Sn. The characterization showed that such catalysts contain alloyed PtSn particles, covered by oxidized forms of tin at the surface, together with ionic tin on the support. Important factors are likely to be (i) the decreased adsorption of C=C bonds on alloyed particles, (ii) the activation of the carbonyl groups on the oxidized Sn ions, (iii) the steric hindrance at the C=C bond of the prostaglandin-type unsaturated ketone, and (iv) the use of a hydrogen transfer agent instead of molecular hydrogen.

ACKNOWLEDGMENTS

We are indebted to the Flemish Government for a grant in the frame of the Bilateral Agreements between Flanders and Romania. We thank Dr. F. Cocu for a gift of the prostaglandin precursor **1** and of reference materials for chromatographic analysis. Part of this work was sponsored by the Belgian Federal Government in the frame of the IAP program "Supramolecular Chemistry and Catalysis."

REFERENCES

1. Poltarzewki, Z., Galvagno, S., Pietropaolo, R., and Staiti, P., *J. Catal.* **102**, 190 (1986).
2. Galvagno, S., Poltarzewki, Z., Donato, A., Neri, G., and Pietropaolo, R., *J. Chem. Soc. Chem. Commun.* 1729 (1986).
3. Galvagno, S., Donato, A., Neri, G., Pietropaolo, R., and Pietropaolo, D., *J. Mol. Catal.* **49**, 223 (1989).
4. Recchia, S., Dossi, C., Poli, N., Fusi, A., Sordelli, A., and Psaro, R., *J. Catal.* **184**, 1 (1999).
5. Torres, G. C., Ledesma, S. D., Jablonski, E. L., de Miguel, S. R., and Scelza, O. A., *Catal. Today* **48**, 65 (1999).
6. de Miguel, S. R., Roman-Martinez, M. C., Jablonski, E. L., Fierro, J. L. G., Cazorla-Amoras, D., and Scelza, O. A., *J. Catal.* **184**, 514 (1999).
7. Arai, M., Takahashi, H., Shirai, M., Nishiyama, Y., and Ebina, T., *Appl. Catal. A* **176**, 229 (1999).
8. de Silva, A. B., Jordao, E., Mendes, M. J., and Fouilloux, P., *Appl. Catal. A* **148**, 253 (1997).
9. Consonni, M., Jokic, D., Yu Murzin, D., Touroude, R., *J. Catal.* **188**, 165 (1999).
10. Hubaut, R., Bonnelle, J. P., Daage, M., *J. Mol. Catal.* **55**, 170 (1989).
11. Aramendia, M. A., Boran, V., Jimenez, C., Marinas, J. M., Porras, A., and Urbano, F. J., *Appl. Catal. A* **172**, 31 (1998).
12. Englisch, M., Jentys, A., and Lercher, J. A., *J. Catal.* **166**, 25 (1997).
13. Szöllösi, G., Torok, B., Szakonyi, G., Kun, I., and Bartok, M., *Appl. Catal. A* **172**, 225 (1998).
14. Szöllösi, G., Torok, B., Baranyi, L., and Bartok, M., *J. Catal.* **179**, 619 (1998).
15. Birchem, T., Pradier, C. M., Berthier, Y., and Cordier, G., *J. Catal.* **161**, 68 (1996).
16. Coq, B., Kumbhar, P. S., Moreau, C., Moreau, P., and Figueras, F., *J. Phys. Chem.* **98**, 10180 (1994).
17. Neri, G., Mercadante, L., Milone, C., Pietropaolo, R., and Galvagno, S., *J. Mol. Catal.* **108**, 41 (1996).
18. Milone, C., Gangemi, C., Ingoglia, R., Neri, G., and Galvagno, S., *Appl. Catal. A* **184**, 89 (1999).
19. Nishiyama, S., Kubota, T., Kimura, K., Tsuruya, S., and Masai, M., *J. Mol. Catal.* **120**, L17 (1997).
20. (a) Aramendia, M. A., Borau, V., Jimenez, C., Marinas, J. M., Porras, A., and Urbano, F. J., *J. Catal.* **172**, 46 (1997); (b) Gallezot, P., and Richard, D., *Catal. Rev.–Sci. Eng.* **40**, 81 (1998); (c) Bartók, M., and Molnár, Á., *in* "Heterogeneous Catalytical Hydrogenation. The Chemistry of Functional Groups. Supplement A3: The Chemistry of Double-Bonded Functional Groups" (Patai, Ed.), p. 843. Wiley, Chichester, UK, 1997; (d) Kun, I., Szöllösi, G., and Bartók, M., *J. Mol. Catal.*, **169**, 235 (2001).
21. Gallezot, P., Giroir-Fendler, A., and Richard, D., *Catal. Lett.* **5**, 169 (1990).
22. Gallezot, P., Blanc, B., Barthomeuf, D., and Pais de Silva, M. I., *Stud. Surf. Sci. Catal.* **84**, 1433 (1994).
23. Parvulescu, V. I., Parvulescu, V., Kaliaguine, S., Endruschat, U., Tesche, B., and Bönnemann, H., *in* "Catalysis of Organic Reactions" (M. E. Ford, Ed.), p. 301. Dekker, New York, 2001.
24. Margitfalvi, J. L., Tompos, A., Kolosova, I., and Valyon, J., *J. Catal.* **174**, 246 (1998).
25. Margitfalvi, J. L., Vanko, Gy., Borbath, I., Tompos, A., and Vertes, A., *J. Catal.* **190**, 474 (2000).
26. Ponec, V., *Appl. Catal. A* **149**, 27 (1997).
27. Brieger, G., and Nestrick, T. J., *Chem. Rev.* **74**, 567 (1974).
28. Johnstone, R. A. W., Wilby, A. H., and Entwistle, I. D., *Chem. Rev.* **85**, 129 (1985).
29. Zassinovich, G., and Mestroni, G., *Chem. Rev.* **92**, 1051 (1992).
30. Goldberg, Y., and Alper, H., *J. Mol. Catal.* **92**, 149 (1994).
31. (a) Mizushima, E., Yamaguchi, M., and Yamagishi, T., *J. Mol. Catal.* **148**, 69 (1999); (b) Szöllösi, G., and Bartók, M., *Catal. Lett*. **59**, 179 (1999); (c) Szöllösi, G., and Bartók, M., *J. Mol. Catal.* **148**, 265 (1999).
32. Collins, P. W., and Djuric, S. W., *Chem. Rev.* **93**, 1533 (1993).
33. Coman, S., Cocu, F., Parvulescu, V. I., De Vos, D. E., and Jacobs, P. A., *Microporous Mesoporous Mate.* **44–45**, 477 (2001).
34. Franke, O., Rathousky, J., Schulz-Ekloff, G., and Zukal, A., *Stud. Surf. Sci. Catal.* **91**, 309 (1995).
35. Xu, J., Luan, Z., He, H., Zhou, W., and Kevan, L., *Chem. Mater.* **10**, 3690 (1998).
36. "Powder Diffraction File." International Centre for Diffraction Data, Newton Square, PA, 1995.
37. Srinivasan, R., De Angelis, R. J., and Davis, B. H., *J. Catal.* **106**, 449 (1987).
38. Chojnacki, T. P., and Schmidt, L. D., *J. Catal.* **129**, 473 (1991).
39. Walbaum, *Z. Metallkd.* **35**, 200 (1943).
40. Schubert, and Pfisterer, *Z. Metallkd.* **40**, 405 (1949).
41. Lieske, H., and Völter, J., *J. Catal.* **90**, 96 (1984).
42. Schubert, M. M., Kahlich, M. J., Feldmeyer, G., Hüttner, M., Hackenberg, S., Gasteiger, H. A., and Behm, R. J., *PCCP* **3**, 1123 (2001).
43. Guczi, L., and Bazin, D., *Appl. Catal. A* **188**, 163 (1999).
44. Adkins, S. R., and Davis, B. H., *J. Catal.* **89**, 371 (1984).
45. Sexton, B. A., Hughes, A. E., and Foger, K., *J. Catal.* **88**, 466 (1984).
46. Llorca, J., de la Piscina, P. R., Fierro, J. L. G., Sales, J., and Homs, N., *J. Catal.* **156**, 139 (1995).
47. Llorca, J., Homs, N., Fierro, J. L. G., Sales, J., and de la Piscina, P. R., *J. Catal.* **166**, 44 (1997).
48. Niemantsverdriet, J., "Spectroscopy in Catalysis." VCH, Weinheim, 1995.
49. Briggs, D., and Seah, M. P. "Practical Surface Analysis by Auger and X-Ray Photoelectron Spectroscopy." Wiley, Chichester, UK, 1985.
50. Knauer, B., and Krohn, K., *Liebigs Ann. Chem.* 677 (1995).
51. Ryndin, Y. A., Santini, C. C., Prat, D., and Basset, J. M., *J. Catal.* **190**, 364 (2000).
52. Delbecq, F., and Sautet, P., *J. Catal.* **152**, 217 (1995).
53. The importance of steric hindrance in the prostaglandin precursor for obtaining selective reduction to the allylic alcohol is evidenced by an experiment with methyl vinyl ketone, which under similar conditions could not be reduced to the corresponding allylic alcohol.